Stem Cell Research & Therapy

RESEARCH

Open Access

Modulation of senescent Lepr$^+$ skeletal stem cells via suppression of leptin-induced STAT3–FGF7 axis activation alleviates abnormal subchondral bone remodeling and osteoarthritis progression

Fu-Hao Yu[1,2,3,4†], Bo-Feng Yin[1,2†], Ming-Yu Liu[1,2,3,4†], Wen-Jing Zhang[1,2†], Zhi-Dong Zhao[5], Lei Wang[5], Xiao-Tong Li[1,2], Pei-Lin Li[1,2], Zhi-Ling Li[1,2], Run-Xiang Xu[1,2,3,4], Li Ding[3,4,7*] and Heng Zhu[1,2,6,7*]

Abstract

Background Recent studies have suggested that targeting senescent cells in joint tissues may alleviate osteoarthritis (OA) progression. However, this strategy encounters significant challenges, partially due to the high degree of cellular heterogeneity in osteoarthritic tissues. Moreover, little information is available on the role of skeletal stem cell (SSC) senescence, as compared to differentiated cells, in OA progression.

Methods In this study, single-cell RNA sequencing (scRNA-seq) on articular cartilages and subchondral bones of the knee joints of mice with post-traumatic osteoarthritis (PTOA) were performed. Further in vivo and in vitro studies were performed to reveal the role and mechanisims of senescent SSCs during the development of OA lesions and progression by microCT, pathological analysis, and functional gain and loss experiments. The one-way ANOVA was used in multiple group data analysis.

Results scRNA-seq and pathological data demonstrated that the leptin receptors (Lepr) positive SSCs underwent cellular senescence during OA progression. In addition, the leptin-Lepr signaling pathway induced signal transducer and activator of transcription 3 (STAT3) expression in SSCs, which consequently augmented the transcription of fibroblast growth factor 7 (FGF7). Further scRNA-seq and in vivo analyses revealed that FGF7 exacerbated abnormal bone remodeling in subchondral bones and OA progression by enhancing bone formation and suppressing bone resorption. In vitro analysis revealed that FGF7 induced the osteogenic differentiation of SSCs but inhibited osteoclastogenesis in a concentration-dependent manner.

[†]Fu-Hao Yu, Bo-Feng Yin, Ming-Yu Liu and Wen-Jing Zhang contributed equally to this work. The work was completed in Beijing, China.

*Correspondence:
Li Ding
dingli7578@163.com
Heng Zhu
zhudingdingabc@163.com
Full list of author information is available at the end of the article

Conclusions In summary, our findings demonstrate that the leptin-Lepr signaling pathway promotes SSC senescence and exacerbates subchondral bone remodeling by activating the STAT3-FGF7 axis during OA progression, which may shed light on novel therapeutic strategies for OA.

Keywords Osteoarthritis, Single-cell sequencing, Skeletal stem cells, Heterogeneity of Cellular senescence, Leptin-Lepr signaling, STAT3-FGF7 axis

Graphical abstract

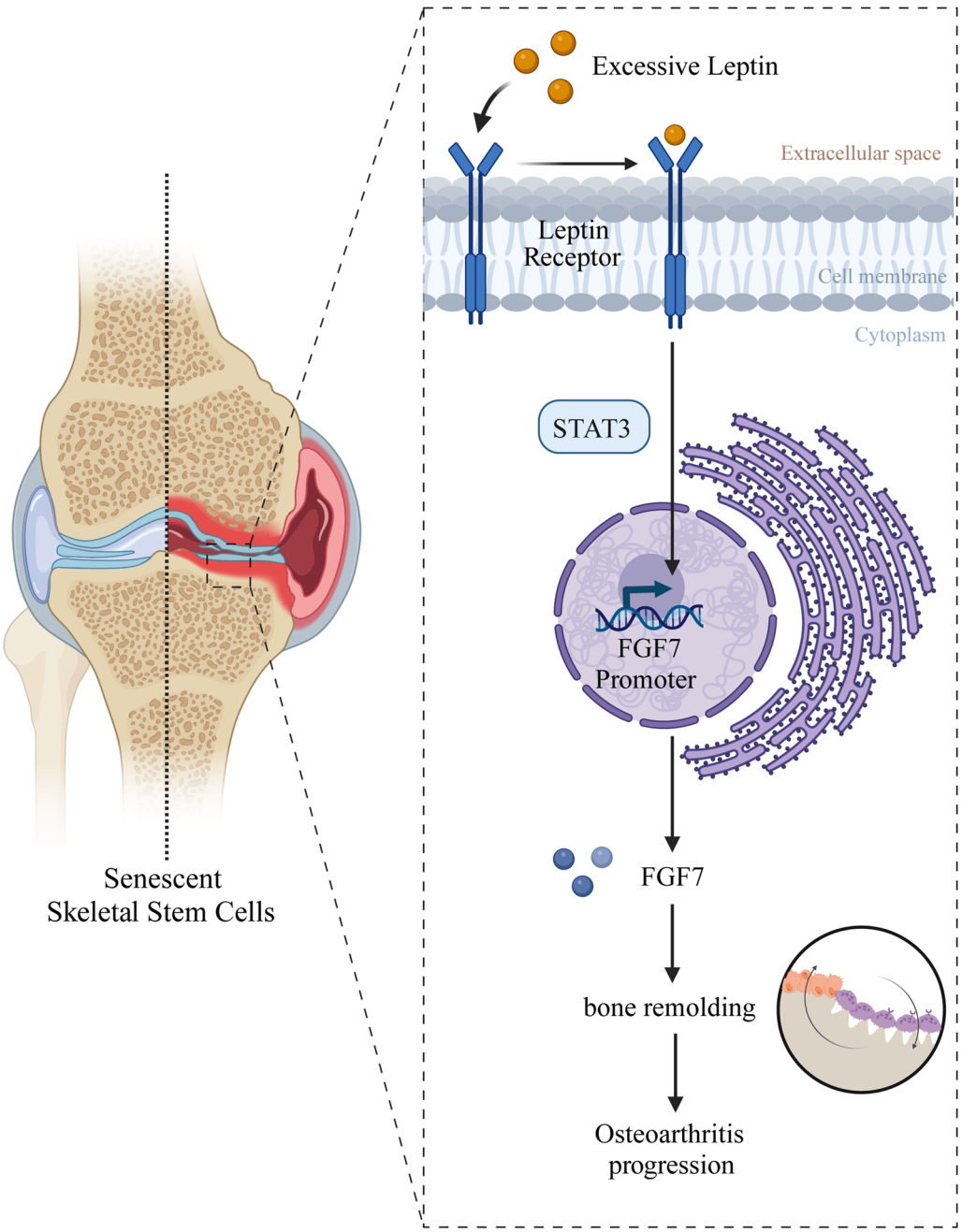

Introduction

Osteoarthritis (OA) is the most common chronic and disabling joint disease with limited therapeutic options [1–3]. Multiple risk factors, such as trauma, genetics, and senescence, induce pathological changes in joints, including synovial inflammation, articular cartilage degradation, and abnormal subchondral bone remodeling, which contribute to OA progression [1–3]. Cellular senescence, characterized by permanent growth arrest and the senescence-associated secretory phenotype (SASP), has recently been identified as a fundamental mechanism contributing to OA pathology [4–6]. Encouragingly, preclinical studies have shown that removing senescent cells or inhibiting SASPs is effective in attenuating OA progression [6–10]. However, senescent cells and SASPs exhibit varying degrees of susceptibility to senolytic drugs, suggesting that single-cell scale studies and specific SASP blockades are important for effectively alleviating osteoarthritic lesions [11, 12]. In addition, most current synolytics target differentiated cells such as chondrocytes and synovial fibroblasts, and the effects of attenuating the senescence of stem cells in joints on the progression of OA remain incompletely understood [13–15].

Skeletal stem cells (SSCs) have recently been identified as tissue-specific stem cells in the skeleton with the potential for osteogenesis and chondrogenesis [16–18]. Previous studies have demonstrated that SSCs contribute to bone development, remodeling, aging, and regeneration [16–20]. Further studies have revealed that SSCs both promote bone formation via osteochondral differentiation and regulate bone resorption by secreting tumor necrosis factor alpha-induced protein 3 (TNFAIP3) to suppress osteoclasts [21]. Moreover, our previous studies revealed that SSCs regulate dendritic cells and macrophages via the release of interleukin-6 and prostaglandin E2 to control inflammatory responses [22, 23]. However, few studies have investigated the role of SSC senescence during OA progression and the underlying mechanisms involved. In addition, owing to the high heterogeneity of SSC subpopulations in joints, examination of the heterogeneity of senescent SSCs is urgently needed. Furthermore, identifying new SSC-specific SASPs and elucidating their role in OA progression are important.

Leptin is a nonglycosylated protein that was originally recognized as an anorexigenic neurohormone that is secreted from white adipose tissues [24]. Further studies revealed that leptin is also derived from the placenta, ovaries, skeletal muscle, bone marrow, and cartilage [25, 26]. In addition to lipid regulation, leptin is associated with multiple physiological processes, including maturation, hematopoiesis, and bone metabolism, by adapting to leptin receptors (Lepr) and regulating Janus kinase/signal transducer and activator of transcription signaling pathways [27]. Numerous studies have demonstrated the effects of leptin in enhancing osteogenesis and endochondral ossification [28, 29]. Furthermore, leptin has been demonstrated to exert a suppressive effect on osteoclastic activity [30]. However, the detailed mechanisms of leptin-Lepr-mediated regulation of subchondral bone remodeling and the therapeutic potential of leptin-Lepr in OA remain to be fully explored.

Fibroblast growth factor 7 (FGF7) is a classic fibroblast growth factor that has a wide range of regulatory functions [31]. Previous studies have demonstrated that FGF7 has potential effects on skeletal development and regeneration, but the underlying mechanisms need to be further elucidated [32, 33]. Liu et al. reported that FGF7 induced the expression and distribution of podoplanin in osteoblasts through connexin43, thereby promoting osteoblast dendrite elongation and functional gap junction formation [34]. Further studies have shown that FGF7 protects osteoblasts from oxidative damage by targeting mitochondria [35]. However, the role of FGF7 in the progression of OA remains completely unknown.

Materials and methods

Human species

Human tibial plateau specimens used in this study were collected from three patients undergoing total knee arthroplasty surgery and with the approval of the Institutional Review Board at the Chinese People's Liberation Army General Hospital (Beijing, China). Informed consent was obtained from all donors. Specific information is provided in Additional Table S1. The human cartilage samples were used for histological assessment, immunohistochemistry (IHC), and Western blotting.

Animals

The work as been reported in line with the ARRIVE guidelines 2.0.

Male C57 mice (8 weeks old, n = 65) were obtained from Vital River Laboratory Animal Technology Co., Ltd. (Beijing, China). The animal research involved in this work was approved by the Institutional Animal Care and Use Committee of Military Medical Sciences (Approval No: IACUC-DWZX-2024-P523). The animals were randomly allocated to control or experimental groups. The mouse studies were carried out in a pathogen-free environment. The laboratory conditions for the mice were as follows: temperature, 22 °C; humidity, 50%; light–dark cycle, 12 h; and water and food were freely available. The Sp7-2A-CreERT2 and Rosa-LSL-Tdtomato mice were

purchased from Shanghai Biomodel Organism Co., Ltd (Shanghai, China). Sp7-Cre/ERT2-Td mice were generated by breeding Rosa-LSL-Tdtomato mice with Sp7-2A-CreERT2 mice. Genotyping was conducted with the primers listed in Table S2.

Chemicals and reagents

Tamoxifen (T5648-1G) was purchased from Sigma–Aldrich (Saint Louis, USA). Allo-aca (HY-P3212), leptin (HY-P7232), FGF7 (HY-P70597), Stattic (HY-13818) and colivelin (HY-P1061) were purchased from MedChemExpress (New Jersey, USA).

ACLT OA animal models

Anterior cruciate ligament transection (ACLT) surgery was performed to generate an OA mouse model. In summary, following anesthesia with pentobarbital sodium, a longitudinal incision was made on the medial aspect of the right/left knee. We subsequently identified the meniscotibial ligament in the intercondylar region and proceeded to transect this ligament; thereafter, we meticulously closed both the joint capsule and the skin. In contrast, in sham-operated mice, although the joint capsule was incised, the meniscotibial ligament was left intact. At 8 weeks after ACLT surgery, mice were euthanized by CO_2 asphyxiation and the whole knee joints were excised, with surrounding soft tissues removed (n = 3). For the genetically engineered mice, prior to surgery, a daily dosage of tamoxifen (Sigma–Aldrich, Saint Louis, USA; T5648) at 100 mg/kg of body weight was administered via intraperitoneal injection to 8-week-old Sp7-Cre/ERT2-Td male mice and their wild-type male littermates over a period of five days.

Intra-articular injection in an OA mouse model

One week after surgery, the mice were anesthetized and intra-articularly injected with adeno-associated virus (AAV) (1×10^{11} v.g. per mL, 10 μL per joint) using 33G needles (Hamilton, Reno, USA; 7803–05). AAV9-Lepr-RNAi, AAV9-Fgf7, AAV9-Fgf7-RNAi, and AAV9-EGFP were constructed by GeneChem (Shanghai, China).

Primary osteoblast progenitor cell isolation and cell culture

The isolation of osteoblast progenitor cells (OPCs) from total knee arthroplasty patients with OA was carried out as previously reported. The human tibial plateau was harvested using a cold phosphate-buffered saline (PBS; Servicebio, Wuhan, China; G4202) washout. Cartilaginous tissues from the superficial layer of the lateral tibial plateau were sliced into small fragments measuring 1–2 mm. To obtain human osteoblast samples, we focused on the subchondral bone region of the tibial plateau, which was similarly cut into 1–2 mm pieces and subsequently placed in α-MEM (Gibco, California, USA; C12571500BT) supplemented with 10% fetal bovine serum (FBS; Pericella, Wuhan, China; 164,210). The cartilage and bone samples were then digested separately in a solution containing 0.1% collagenase II (Sigma-Aldrich, Saint Louis, USA; V900892) at 37 °C for two hours. Following digestion, both types of tissue were transferred to 25-cm^2 tissue culture plates and incubated at 37 °C in an atmosphere enriched with 5% CO_2. The culture medium was refreshed every three days to support cell growth. Unless otherwise specified, stem cells at passages 3–4 were utilized for both in vivo and in vitro studies.

Differentiation assays of SSCs

For osteogenic and chondrogenic differentiation, SSCs were cultured in osteogenic induction medium (Cyagen, California, USA; HUXMA-90021) and chondrogenic induction medium (Cyagen, California, USA; HUXMA-90041), respectively. The cells were seeded in 24-well plates at a density of 3×10^4 cells per well. The induction medium was replaced every three days. Following 14 d of osteogenic and chondrogenic induction, the samples were subjected to alkaline phosphatase (ALP) staining (Sigma-Aldrich, Saint Louis, USA; 386A-1KT) to assess bone formation and toluidine blue staining (Sigma-Aldrich, Saint Louis, USA; 198,161) to evaluate cartilage formation. For adipogenic differentiation, SSCs were cultured in adipogenic induction medium (Cyagen, California, USA; HUXMX-90031) in 24-well plates at a density of 5×10^4 cells per well; the induction medium was also replaced every three days. Oil Red O staining (Sigma-Aldrich, Saint Louis, USA; O1391) was conducted on Day 14 following adipogenic induction to evaluate the samples.

qPCR analysis

Total RNA extraction and reverse transcription were performed using the Tissue RNA Purification Kit Plus (ES Science, Shanghai, China; RN002plus) and PrimeScript RT Master Mix (Takara, Shiga, Japan; RR036A), respectively. mRNA expression was detected by using a SYBR Green PCR kit (Sigma–Aldrich, Saint Louis, USA; QR0100) and a 7500 Real-Time PCR Detection System (Thermo Fisher Scientific, Waltham, MA, USA; 4,351,105). The primer sequences are listed in Tables S3 and S4.

Western blot assay

Total protein from bone tissues subjected to different treatments was collected using a commercial kit (Proteintech, Wuhan, China; PK10021). The proteins were subsequently subjected to electrophoresis on a 10% SDS

polyacrylamide gel and transferred onto Polyvinylidene Fluoride (PVDF) membranes (Millipore, Burlington, MA, USA; IPVH00010). The membranes were blocked for 1 h with 5% nonfat dry milk and incubated with primary antibodies. The following primary antibodies were used: GAPDH (Proteintech, Wuhan, China; 10,494-1-AP, 1:5000), STAT3 (Proteintech, Wuhan, China; 10,253-2-AP, 1:3000), and FGF7 (Affinity, Cincinnati, OH, USA; DF13342, 1:1000). The following secondary antibodies were used: goat anti-rabbit IgG (H + L) and HRP (Affinity, Cincinnati, OH, USA; S0001, 1:5000). The membrane was incubated overnight at 4 °C with primary antibody and for 1.5 h with secondary antibody and then visualized with an eECL Western blot Kit (CWBIO, Jiangsu, China; CW0049M) with a Tanon-5200 (Tanon, Shanghai, China).

Histology, immunofluorescence, and immunohistochemistry

Knee joints freshly dissected from the mice were fixed for 48 h in 4% paraformaldehyde at 4 °C and then decalcified for two weeks in 10% Ethylenediaminetetraacetic acid (pH 7.2–7.4). The tissues were embedded in paraffin and sectioned continuously (4 mm thick), and serial sections were stained with safranin-O/Fast Green. We quantified degeneration of the articular cartilage with the OARSI scoring system. COL II (Servicebio, Wuhan, China; GB150010-100, 1:200), P21 (Proteintech, Wuhan, China; 10,355-1-AP, 1:200), IL-6 (Servicebio, Wuhan, China; GB11117-100, 1:200), IL-1β (Proteintech, Wuhan, China; 26,048-1-AP, 1:200), FGF7 (Affinity, Cincinnati, OH, USA; DF13342, 1:100), and Tartrate-resistant acid phosphatase (TRAP) (Servicebio, Wuhan, China; G1050-50 T) were detected by IHC. The expression levels of Lepr, Grem1, and P21 were determined by immunofluorescence (IF). The following primary and secondary antibodies were used: Lepr (Proteintech, Wuhan, China; 20,966-1-AP, 1:100), Grem1 (Affinity, Cincinnati, OH, USA; DF15419, 1:100), P21 (Proteintech, Wuhan, China; 10,355-1-AP, 1:100), HRP-labeled goat anti-rabbit IgG (Servicebio, Wuhan, China; GB23303), and Alexa Fluor® 488-labeled goat anti-rabbit IgG (Servicebio, Wuhan, China; GB25303). An inverted microscope (Olympus, Tokyo, Japan; CKX53) equipped with a cooled CMOS camera (Tucsen, Fujian, China; FL-20BW) was used for image acquisition. Semiquantitative analyses of IHC and IF staining were performed using ImageJ software (version 1.53) as described previously.

Micro-CT analysis

The knee joints were dissected and fixed in 4% paraformaldehyde for 48 h at 4 °C and scanned on a micro-CT scanner (Revvity, Waltham, MA, USA; QuantumGX2) at a resolution of 5.12 μm (90 kV, 88 mA, integrated for 14 min). The scanned images were evaluated at the same threshold to allow three-dimensional structural rendering of each sample. 3D image reconstruction and visualization were conducted using CTvox software (version 2.0.0). Data analysis was performed with CTAn software (version 1.18).

Luciferase reporter assays

293 T cells were cotransfected with 3′ UTR luciferase reporter constructs (pGL3-Basic vector, pGL3-FGF7-WT-Promoter, pGL3-FGF7-1106/1114-Mutant-Promoter), pcDNA3.1(+) (vector and STAT3), and Renilla luciferase using jetPRIME® (Polyplus, Illkirch-Graffenstaden, France; 114-15) for 48 h. The STAT3 + pGL3-FGF7-WT-Promoter group was supplemented with culture medium containing 50 μg/mL colivelin (MCE, New Jersey, USA; HY-P1061), and samples were collected 30 min after reagent addition. Samples from the other groups were collected directly. Luciferase activity was measured using a Dual-Luciferase Reporter Assay Kit (Beyotime, Shanghai, China; RG028) and a microplate reader (Thermo Fisher Scientific, Waltham, MA, USA; Varioskan LUX).

Preprocessing of scRNA-seq data

Gene expression matrices for the sequenced samples were produced using the Cell Ranger (10X Genomics, Pleasanton, California, USA; v7.2) count function by aligning raw sequencing FASTQ files to the mm10 reference genome via the STAR algorithm. We removed low-quality cells that had > 6250 or < 600 expressed genes or > 10% UMIs derived from the mitochondrial genome and removed potential cell doublets using the DoubletFinder [36] R package as the dropout effect of 10 × data.

Single-cell RNA-seq data analyses

We downloaded public single-cell RNA-seq data from NCBI (GSE231755). The Seurat [37] R package (version 5.1.0) was used to perform subsequent data analysis, including normalization, scaling, principal component analysis, uniform manifold approximation and projection (UMAP) dimension reduction, and visualization of gene expression. To cluster cells, graph-based clustering was performed based on each cell gene expression profile via the Find Clusters function. The visualization of cells was performed via a UMAP algorithm using the RunUMAP function in Seurat. All marker functions were used to verify the marker genes of each cluster. Differentially expressed genes (DEGs) were identified via the Find Markers function in Seurat. The significant DEG thresholds were a P value of < 0.05 and a |log2-fold change| > 0.5.

The cell types were annotated based on known canonical marker genes and DEGs, which were calculated with the FindAllMarker function using default parameters provided by Seurat. Gene Ontology (GO) enrichment and Kyoto Encyclopedia of Genes and Genomes (KEGG) pathway enrichment analyses of DEGs were conducted using R.

Trajectory analysis

We utilized the Monocle [38] algorithm to elucidate cell differentiation trajectories. Dimensionality reduction and trajectory construction were conducted on the selected genes using the reduceDimension and plot_cell_trajectory functions. A heatmap was generated to visualize individual gene expression along a pseudotime continuum employing the plot_pseudotime_heatmap function.

CellChat analysis

To explore potential intercellular crosstalk networks, we assessed ligand–receptor distribution and expression levels in SSCs and other subpopulations via a standard pipeline implemented in R using the CellChat [39] R package, as previously reported.

Statistical analysis

Analysis of the results and graph construction was performed using GraphPad Prism 8.0 software. A one-way ANOVA was used to determine the significance of comparisons between multiple groups. A $P<0.05$ indicated statistical significance ($^{*}P<0.05$, $^{**}P<0.01$, and $^{***}P<0.001$).

Results

SSCs underwent cellular senescence in the knee joints of PTOA mice during OA progression

To explore the heterogeneity of cellular senescence in the knee joints of PTOA mice, we used anterior cruciate ligament transection (ACLT) to establish a PTOA mouse model (Figure S1A–D) and performed droplet-based scRNA-seq of $Lin^{-}CD45^{-}Ter119^{-}$ stromal cells and $CD45^{+}$ immune cells isolated from the epiphysis and part of the diaphysis of the tibia. In addition, we integrated data from public sources, including the infrapatellar fat pad and synovium, which were sampled at the same time points during OA progression (Fig. 1A). After cell filtering, we obtained gene expression profiles for 96,360 cells from 12 samples (Figure S1E). After pooling, the cells were divided into two major clusters (immune cells and stromal cells), including 9 immune cell types and 9 stromal cell types (Fig. 1B and S1F). Furthermore, cell trajectory analysis was conducted, which corroborated the hypothesis that SSCs function as upstream progenitors in the osteogenic lineage (Figure S2A, B). Additionally, the expression of several stromal genes, including Lepr, Gremlin 1 (Grem1), paired related homeobox 1 (Prrx1), bone gamma-carboxyglutamate protein (Bglap), and cadherin 5 (Cdh5), demonstrated the existence of discrete differentiation trajectories among the stromal cells (Figure S2C, D). As shown in Fig. 1C, osteoblastic lineage cells constituted the primary component of the bone cells. Interestingly, cartilage progenitor cells (CPCs), fibroblasts (FCs), endothelial cells (ECs), and pericytes were also distributed in the synovial membrane and fat pad (Fig. 1C). Notably, there was an increase in the number of SSCs and OPCs in the initial phase of the knee joint in PTOA mice, which subsequently decreased during OA progression. In contrast, the number of osteoblasts (OBs) decreased in the early stages of OA but increased in the late stages. As OA progressed, there was a gradual decrease in the proportion of immune cells. In the eighth week after ALCT, there was a significant reduction in the proportion of immune cells, which may be attributed to the development of pronounced bone hardening in the later stages of the disease (Fig. 1C).

Cellular senescence has been classically described as stable cell cycle arrest in response to stress. By calculating cell cycle phase scores based on canonical markers, we found that the number of bone stromal cells in the G1 phase increased and the number in the S phase decreased during OA progression (Fig. 1D). Additionally, stromal cells presented elevated levels of cyclin-dependent kinase inhibitor 1A (Cdkn1a, also known as P21), a crucial cell cycle inhibitor, during OA progression (Fig. 1E). Moreover, the expression of numerous genes associated with senescence, including cyclin-dependent kinase inhibitor 2A (Cdkn2a, also known as P16), Interleukin-1β (IL-1β), and cellular tumor antigen p53 (P53), increased during OA progression (Figure S2E–G). To explore the effects of cellular senescence on different cell populations,

(See figure on next page.)

Fig. 1 Single-cell sequencing revealed that skeletal stem cells underwent cellular senescence in knee osteoarthritis. **A** Schematic overview of the scRNA-seq workflow. **B** UMAP plots showing integrated analysis of bone stromal, immune, and synovial cells. The cells are colored according to their clusters. **C** Proportions of different cell clusters across different sources, including bone stromal cells, bone immune cells, and synovial cells, at different points in the progression of OA. **D** Stacked bar charts showing the cell cycle status of all samples. **E** mRNA levels of P21 in all samples. **F** Scoring of the senescent gene set (SenMayo) in different cell clusters. **G**, **H** GO terms enriched in upregulated (**G**) and downregulated (**H**) genes

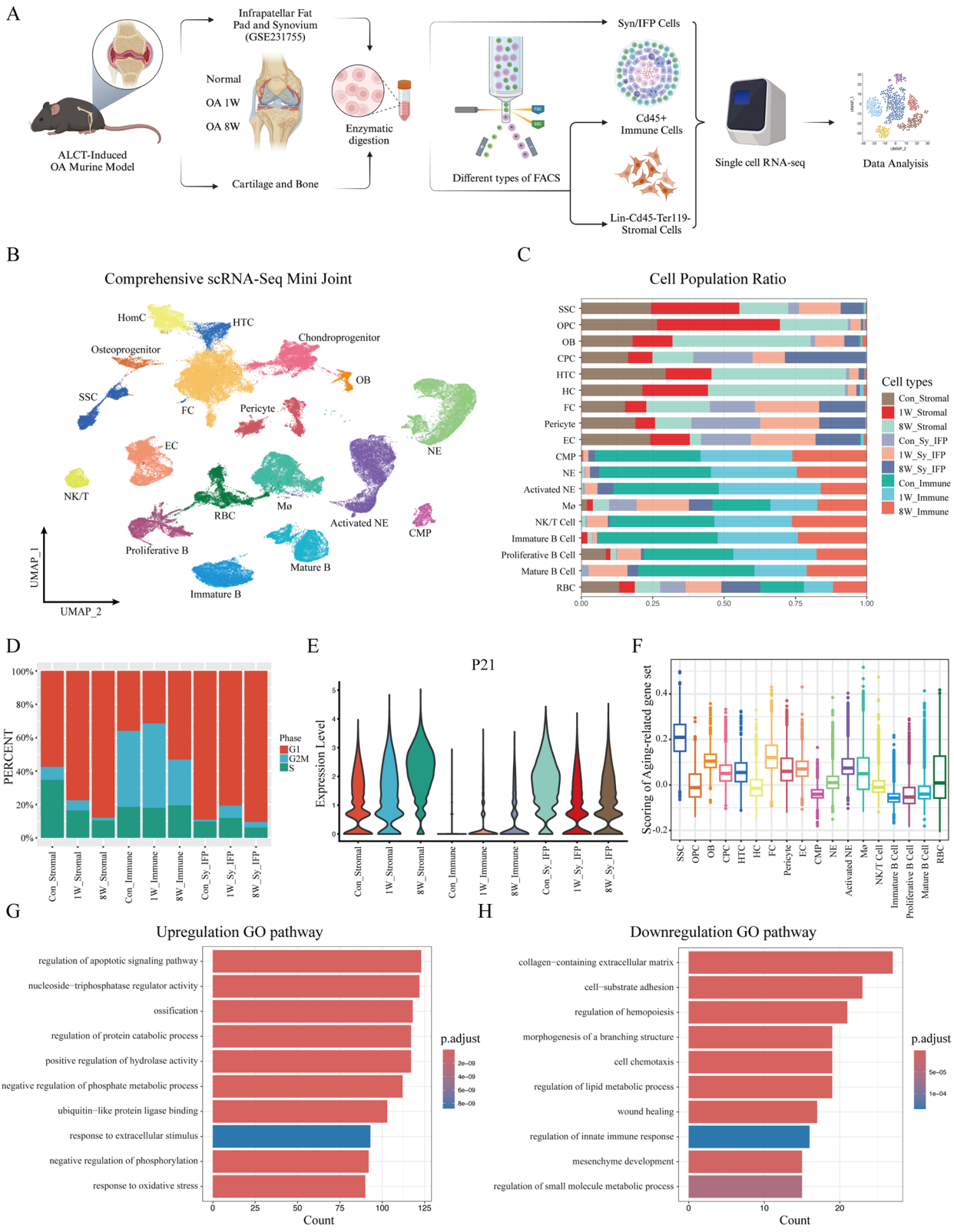

Fig. 1 (See legend on previous page.)

we used a gene set (SenMayo) capable of identifying senescent cells across tissues and species. Thus, the enrichment of cellular senescence in SSCs was revealed (Fig. 1F). In addition, we also showed that some of the genes that regulate inflammation and senescence in the gene set were upregulated in SSCs with the progression of OA (Figure S2H). GO and gene set enrichment analysis (GSEA) revealed alterations in the cell differentiation and metabolism of SSCs, which suggested that the SSCs were undergoing a process of cellular senescence and were potentially involved in senescence of the skeletal system (Fig. 1G, H and S2I).

To further verify the bioinformatics findings, we performed wet experiments to validate that bone stromal cells, specifically SSCs, promote cell senescence and accelerate osteochondral lesions in OA mice. As OA progressed, P21 expression in the osteochondral tissues of the PTOA knee joints gradually increased (Fig. 2A). As shown in Fig. 2B, the positive area of P21 immunohistochemical staining reached 29.9% of the total area at 8 weeks post-ACLT (Fig. 2B). The expression of IL-1β and interleukin-6 (IL-6), which are well-known SASPs, increased in a manner similar to that of P21 during the progression of OA (Fig. 2C–F). Further immunofluorescence data revealed that the number of $Lepr^{+}P21^{+}$ cells and $Grem1^{+}P21^{+}$ cells significantly increased in the subchondral bones of PTOA mice (Fig. 2G–J), which suggested that SSCs undergo cellular senescence during OA progression. To further investigate whether SSC senescence occurs in human OA, tibial plateau specimens were collected from patients undergoing total knee arthroplasty surgery (Table S1). The expression of P21 and IL-6 in the cartilage and subchondral bone regions on the more damaged side of OA tissues (OA grade II-III) was significantly greater than that on the less damaged side of the joint (OA grade 0-II), which is consistent with previous findings in PTOA mice (Fig. 2K–N).

In summary, bone stromal cells, particularly SSCs, undergo significant cell senescence during the progression of OA.

Inhibition of the leptin-Lepr signaling pathway mitigated SSC senescence and OA progression

Although $Lepr^{+}$ SSCs were found to be subject to cell senescence during OA progression, the underlying mechanisms remain elusive. Some adipokines, including leptin, have been demonstrated to exacerbate cartilage erosion and promote inflammatory pathways in joint disorders. In the present study, the data from the scRNA-seq analysis indicated that lipid metabolism is aberrant in senescent SSCs (Fig. 3A), with the activation of numerous downstream pathways of the leptin-Lepr signaling cascade (Fig. 3B). Further mRNA expression analysis of osteochondral tissues from OA patients (Fig. 3C) and PTOA mice (Fig. 3D) confirmed a significant increase in leptin during OA progression. To explore the hypothesis that aberrantly activated leptin-Lepr signaling accelerates the progression of OA, in vivo leptin blockade experiments were performed (Fig. 3E). AAV9-Lepr-Down (1×10^{11} v.g. per mL, 10 μL per joint) was administered into the joint cavity of OA mice at 1 week, and osteochondral tissue from the knee joints was harvested at 8 weeks post-ACLT (Fig. 3E). To further explore the potential role of the leptin-Lepr pathway in OA progression, a specific inhibitor targeting the leptin-Lepr pathway, Allo-aca, was given to PTOA mice via intra-articular injection (Fig. 3E). As shown in Fig. S3A, obvious enhanced green fluorescent protein signals were observed in articular chondrocytes and osteoblasts 1 month after intra-articular injection. In addition, the results of the mRNA analysis further confirmed that AAV injection resulted in significant knockdown of the Lepr gene in the knee osteochondral tissues of PTOA mice (Figure S3B).

Compared with the vehicle and PBS, intra-articular injection of Lepr-Down AAV or Allo-aca effectively attenuated cartilage damage (Fig. 3F, G). Consistent with the histology results, the area of collagen type II (COL II) was dramatically increased in the Lepr-Down and Allo-aca groups (Fig. 3H, I). Furthermore, taking into account the influence of AAV on Lepr gene expression, we investigated the trend of senescence changes in SSCs through costaining for Grem1 and P21. The results

(See figure on next page.)

Fig. 2 Bone stromal cells, particularly SSCs, are significant markers of senescence in osteoarthritis. **A**, **C**, **E** Representative images of P21 (**A**), IL-1β (**C**), and IL-6 (**E**) IHC in articular cartilage and subchondral bone at different points in the progression of OA. Scale bar, 100 μm. **B**, **D**, **F** Quantitative analysis of the P21 (**B**), IL-1β (**D**), and IL-6 (**F**) areas in articular cartilage and subchondral bone (n = 3). **G** IF staining of Lepr and P21 in mouse subchondral bones in various treatment groups. The white arrows indicate P21-positive cells. Scale bar, 100 μm. **H** Proportion of $Lepr^{+}P21^{+}$ cells among $Lepr^{+}$ cells (n = 3). **I** IF staining of Grem1 and P21 in the subchondral bones of mice in various treatment groups. The white arrows indicate the double-positive cells. Scale bar, 100 μm. **J** Proportion of $Grem1^{+}P21^{+}$ cells among $Grem1^{+}$ cells (n = 3). **K**, **L** Representative images of P21 (**K**) and IL-6 (**L**) IHC in the articular cartilage and subchondral bone of OA human samples. The N side represents the less severely diseased side of the source joint, whereas the O side represented the more severely diseased side of the joint. Scale bar, 100 μm. **M**, **N** Quantitative analysis of P21 (**M**) and IL-6 (**N**) levels in articular cartilage and subchondral bone (n = 3). Quantitative analyses were conducted using the IHC Profiler plug-in for Image J. All data are presented as the mean ± S.D. *$P < 0.05$; **$P < 0.01$; ***$P < 0.001$; ns, not significant

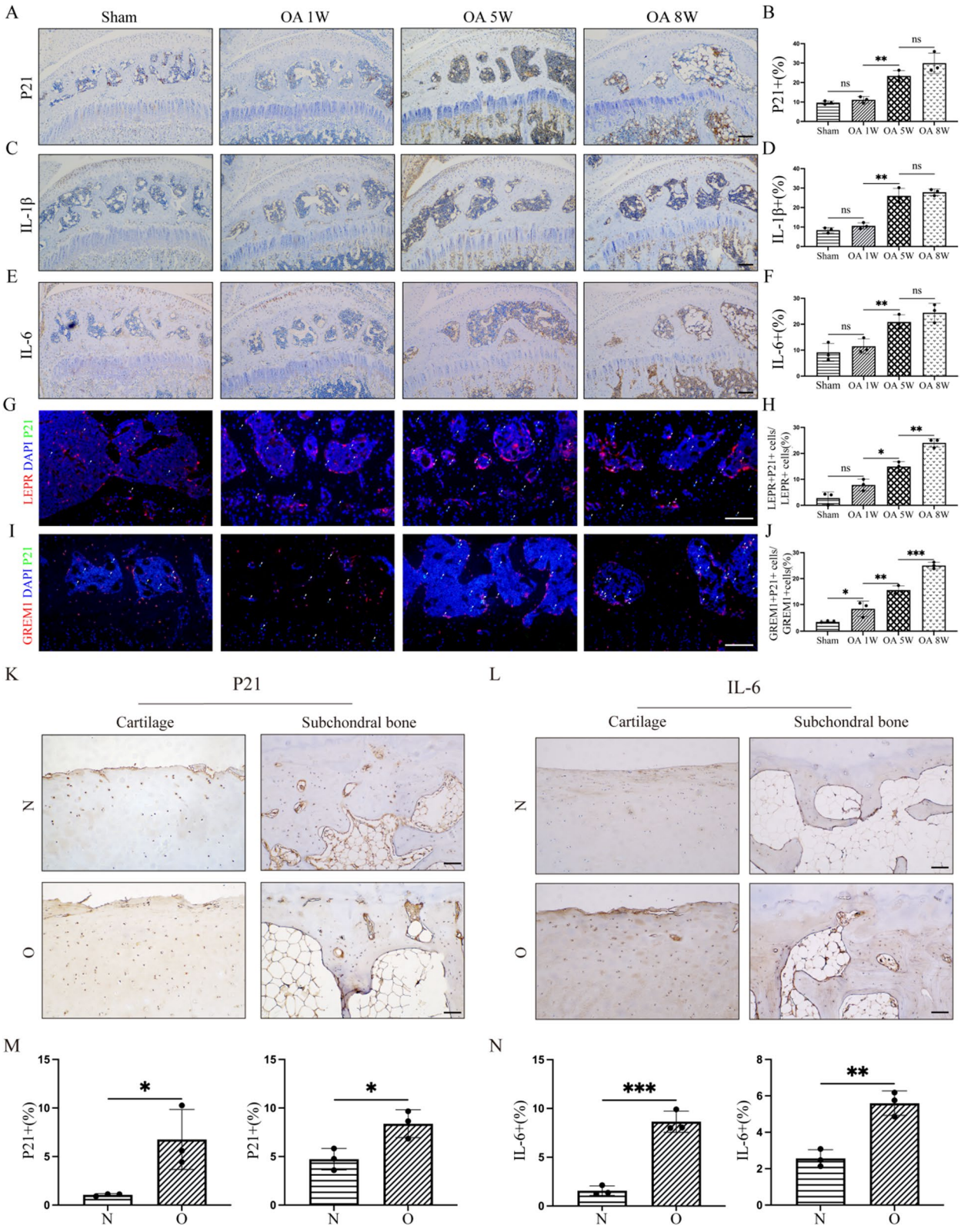

Fig. 2 (See legend on previous page.)

revealed that the proportion of double-positive cells expressing both Grem1 and P21 was reduced after leptin-Lepr pathway blockade (Fig. 3J, K). Moreover, 3D reconstructed micro-CT data of the mouse knee joints showed that treatment with AAV9-Lepr-Down or Allo-aca significantly alleviated the articular lesions and ameliorated the osteosclerosis of subchondral bones (Fig. 3L). Furthermore, bone microarchitecture parameters, including Bone volume fraction (BV/TV) and subchondral bone plate thickness (SBP.th), were determined. The data indicated that BV/TV and SBP.th tended to decrease following the inhibition of the leptin-Lepr pathway. These findings suggest that the leptin-Lepr pathway may promote osteogenic hyperactivity in OA (Fig. 3M, N).

In conclusion, the aforementioned experiments provide evidence that the leptin-Lepr signaling pathway is associated with the senescence of SSCs and contributes to the process of abnormal subchondral bone remodeling in OA.

The expression of STAT3 and FGF7 in SSCs increased during OA progression

Although the leptin-Lepr pathway has been shown to be involved in SSC senescence and OA progression, the underlying mechanisms remain to be elucidated. TargetScan and the protein–protein interaction network database STRING were used to analyze Lepr-targeted proteins (Fig. 4A). The expression of STAT3, which has been reported to be involved in skeletal development and bone homeostasis by regulating osteogenesis was observed to escalate in correlation with the progression of OA (Fig. 4B). Furthermore, the mRNA expression of STAT3 was assessed using QPCR. The data further revealed that the expression of STAT3 was significantly elevated in both OA mice and human samples compared with that in the control group (Fig. 4C, D).

To gain insight into the alterations in specific signaling pathways within SSCs during the progression of cellular senescence and OA, a CellChat analysis was conducted. The results showed that the SSC population was the strongest receiver and sender of signals across all enriched signals (Fig. 4E). The specific signals that contributed to both incoming and outgoing signaling networks were identified and visualized as a heatmap (Fig. 4F). Additionally, the receptor pairs between SSCs and other types of cells in signaling pathways were explored (Figure S4A). The relative significance of the SSCs in the fibroblast growth factor (FGF) (Fig. 4G), C-X-C motif chemokine ligand (CXCL) (Figure S4B), secreted phosphoprotein 1 (SPP1) (Figure S4C), and bone morphogenetic protein (BMP) (Figure S4D) signaling networks was evaluated. The results showed that these pathways were significantly enriched in SSCs, which suggested potential correlations with functional roles. Notably, FGF7 expression was enriched in SSCs (Fig. 4G) during OA progression, and its downstream interactions primarily involved the fibroblast growth factor receptor (Fgfr) family (Fig. 4H). As illustrated in the violin plot of Fig. 4G, the FGF7 gene is specifically expressed in the SSC population whereas the FGF2 gene is expressed in the HC, HTC, and OB populations. Thus, the FGF7 gene was selected as a target for intervention because the aim of the current study mainly focus on the possible roles of SSC populations during OA progression. Moreover, the interaction between Fgf7 and its downstream receptors Fgfr1 and Fgfr2 progressively increased during OA progression (Fig. 4I). The analysis demonstrated that SSCs were a significant source of FGF signaling, and the intensity of FGF signaling increased during the progression of OA. The results of IHC confirmed that FGF7 expression was elevated in correlation with the progression of OA in both OA mice (Fig. 4J, K) and human samples (Fig. 4L, M). qPCR results also showed that the mRNA expression level of FGF7 progressively increased

(See figure on next page.)

Fig. 3 Inhibition of the leptin-Lepr signaling pathway mitigated SSC senescence and OA progression. **A** GO enrichment of pathways associated with significantly upregulated genes (p.adjust < 0.05) in the normal versus OA 8W groups. **B** GSEA enrichment of pathways associated with significantly upregulated genes (p.adjust < 0.05) in the normal versus OA 8W groups. **C**, **D** mRNA levels of leptin in osteochondral tissues from human (**C**) and OA mice (**D**) samples. The N side represents the less severely diseased side of the source joint, whereas the O side represents the more severely diseased side of the joint. **E** Schematic of the experimental design. The mice were subjected to ACLT surgery and received intra-articular treatment (n = 3). **F**, **G** Representative images of safranin O/Fast Green staining and OARSI grades of the mice that received different treatments at 8 weeks after ALCT surgery. Scale bars, 100 μm. **H** Representative images of COL II IHC in the articular cartilage and subchondral bone of mice that received different treatments at 8 weeks after ALCT surgery. Scale bar, 100 μm. **I** Quantitative analysis of the COL II area in articular cartilage and subchondral bone. **J** IF staining of Grem1 and P21 in the subchondral bones of mice that received different treatments at 8 weeks after ALCT surgery. The white arrows indicate P21-positive cells. Scale bar, 100 μm. **K** Proportion of $Grem1^{+}P21^{+}$ cells among $Grem1^{+}$ cells. **L** Micro-CT scans of knee joints from various treatment groups after ALCT surgery. **M**, **N** Microarchitectures of tibial subchondral bones showing BV/TV (**M**) and SBP.th (**N**). Quantitative analyses were conducted using the IHC Profiler plug-in for ImageJ. All data are presented as the mean ± S.D. *$P < 0.05$; **$P < 0.01$; ***$P < 0.001$; ns, not significant

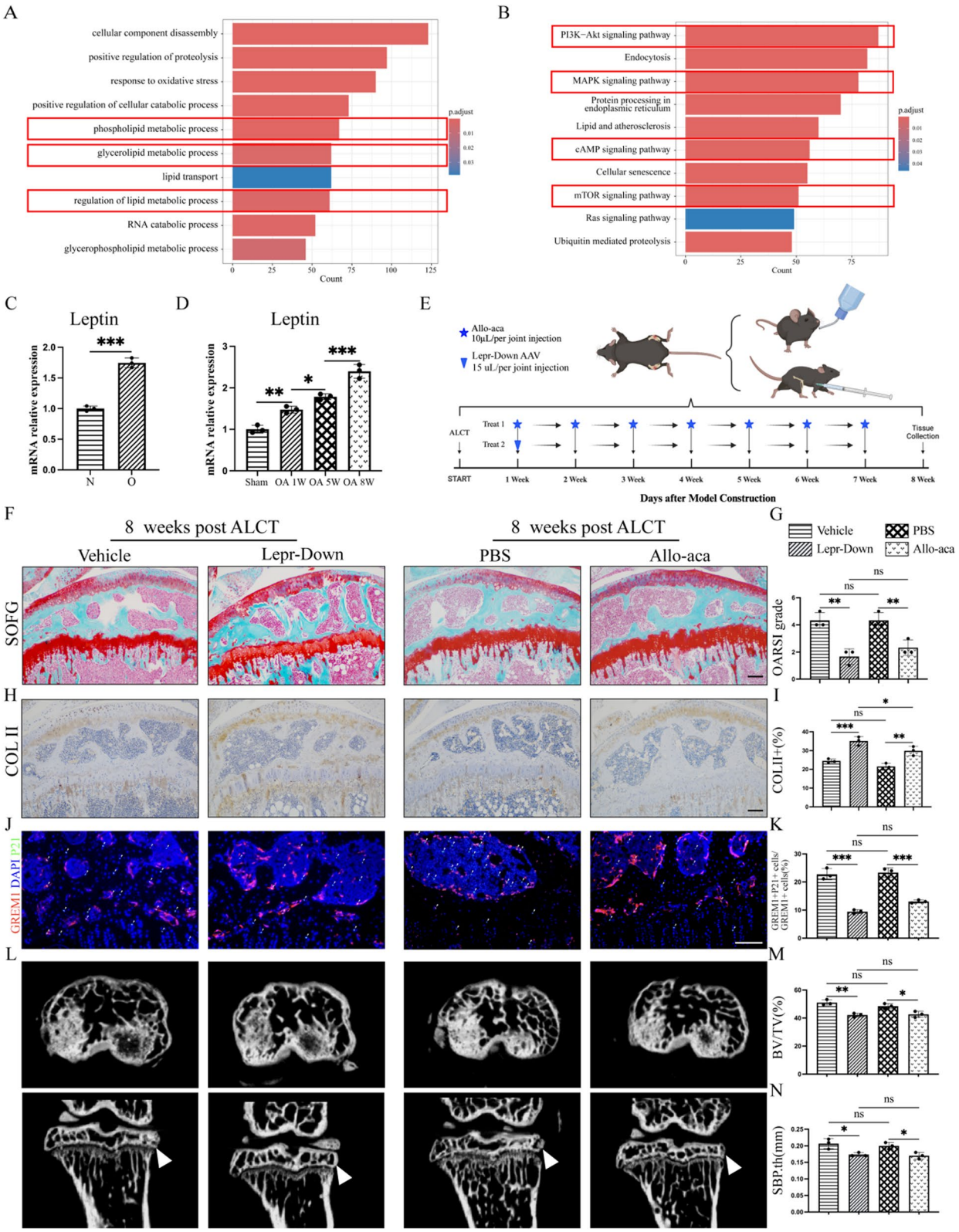

Fig. 3 (See legend on previous page.)

with increasing OA in both murine and human OA samples (Fig. 4N, O).

In conclusion, the aforementioned data indicate that SSCs constitute a significant subpopulation involved in signal transduction within the context of OA by engaging in various intercellular interactions. Furthermore, the expression of FGF7 in SSCs was found to correlate with the progression of OA. In addition, FGF7 expression in SSCs may be regulated by STAT3, which is situated downstream of the leptin-Lepr signaling pathway.

Leptin-Lepr signaling enhances the transcription of FGF7 via *STAT3 activation*

To explore the detailed mechanisms by which FGF7 elevation is mediated by leptin-Lepr signaling in senescent SSCs, the relevance of STAT3 and elevated FGF7 expression were further investigated using numerous osteoblastic cell lines, including an osteosarcoma cell line (MG-63), a human fetal osteoblastic cell line (hFOB) and a human tibial plateau-derived osteoblast progenitor cell line (OPC) (Figure S5A). Our findings indicated that leptin promoted the upregulation of STAT3 and FGF7 expression in a dose-dependent manner across a range of cell lines (Fig. 5A). Furthermore, leptin (50 ng/mL) alongside different concentrations of a STAT3 inhibitor (Stattic) was added to the cell cultures to ascertain whether the increase in FGF7 by leptin was mediated through STAT3. The WB results indicated that the expression levels of both STAT3 and FGF7 decreased in a dose-dependent manner in the presence of Stattic (Fig. 5B).

Although the aforementioned study indicated that STAT3 could influence FGF7 expression, it remained uncertain whether this regulation had direct or indirect effects. Subsequent analysis using JASPAR (a transcription factor binding profile database) suggested that STAT3 may bind to the promoter region of FGF7. In addition, a putative STAT3 binding site in the promoter region of FGF7 was identified (Fig. 5C, D). The overexpression of STAT3 in 293 T cells harboring the FGF7-WT promoter increased luciferase activity, whereas mutation of the 9 bp core sequence of the STAT3 binding site (Mutant) decreased luciferase activity in parallel (Fig. 5E–G). To explore whether the phosphorylation of STAT3 contributes to FGF7 expression, colivelin, an agonist of the STAT3 signaling pathway (Fig. 5E, F), was included in the present study. The results indicated that the addition of colivelin significantly increased luciferase activity compared with that in the group overexpressing STAT3 alone (Fig. 5G), which suggests that phosphorylated STAT3 may contribute to FGF7 regulation, but further investigations are needed.

Overall, our data suggest that STAT3, one of the downstream signaling pathways of the leptin-Lepr pathway, directly regulates FGF7 expression in osteoblastic cells partly by regulating FGF7 transcription.

FGF7 regulated bone remodeling during OA progression

Recent studies have demonstrated the critical role of FGF7 in the growth and differentiation of osteocytes as well as in the formation of cell junctions. Additionally, we confirmed its osteogenic-promoting effects on MG-63, hFOB, and OPC cells (Figure S5B). To further investigate the impact of upregulated FGF7 in OA, we conducted an experiment utilizing intra-articular injections of AAVs that either overexpressed or silenced FGF7 (Fig. 6A). An identical AAV9 vector was used for transfection (Figure S3A). After intra-articular injection of AAV, the OARSI grade decreased by 1.9-fold in the FGF7-Down group compared with that in the Vehicle group (Fig. 6C, G). The area of the COL II$^+$ region (Fig. 6D, H) in the FGF7-Down group was greater than that in the Vehicle group. These changes may be due to the accelerated degradation of the matrix by FGF7-FGFR1 signaling in articular chondrocytes. In addition, qPCR analysis indicated that FGF7 also upregulated osteogenic markers, including runt-related transcription factor 2 (RUNX2), specificity protein 7 (SP7), and SPP1 (Fig. 6I, J). To further elucidate the role of FGF7 in bone formation, we used

(See figure on next page.)

Fig. 4 The expression of STAT3 and FGF7 in SSCs increased during OA progression. **A** Schematic of the protein interaction diagram related to Lepr. **B** mRNA levels of STAT3 in SSCs at different time points after ALCT. **C**, **D** QPCR analysis of the expression levels of STAT3 in OA mouse (**C**) and human (**D**) samples. The N side represents the less severely diseased side of the s source joint, whereas the O side represents the more severely diseased side of the joint. **E** CellChat analysis was performed to investigate the cell–cell communication patterns between clusters in articular cartilage. The overall outgoing and incoming signal strengths of each cluster were visualized in a scatter plot. **F** The relative strength of all enriched signals (outgoing and incoming) across various clusters was visualized in a heatmap. **G** Violin plot showing the expression of canonical markers in the FGF signal. **H** FGF signaling pathway-associated ligand–receptor. **I** Circle plots showing the dynamic alterations in the interaction networks between Fgf7 and Fgfr1 as well as between Fgf7 and Fgfr2. **J**, **L** Representative images of FGF7 IHC in articular cartilage and subchondral bone in OA mouse (**J**) (n = 3) and human (**L**) (n = 2) samples. Scale bar, 100 μm. **K**, **M** Quantitative analysis of the FGF7 area in articular cartilage and subchondral bone in OA mouse (**K**) and human (**M**) samples. **N**, **O** QPCR analysis of the expression levels of FGF7 in OA mouse (**N**) and human (**O**) samples. Quantitative analyses were conducted using the IHC Profiler plug-in for ImageJ. All data are presented as the mean ± S.D. *$P < 0.05$; **$P < 0.01$; ***$P < 0.001$; ns, not significant

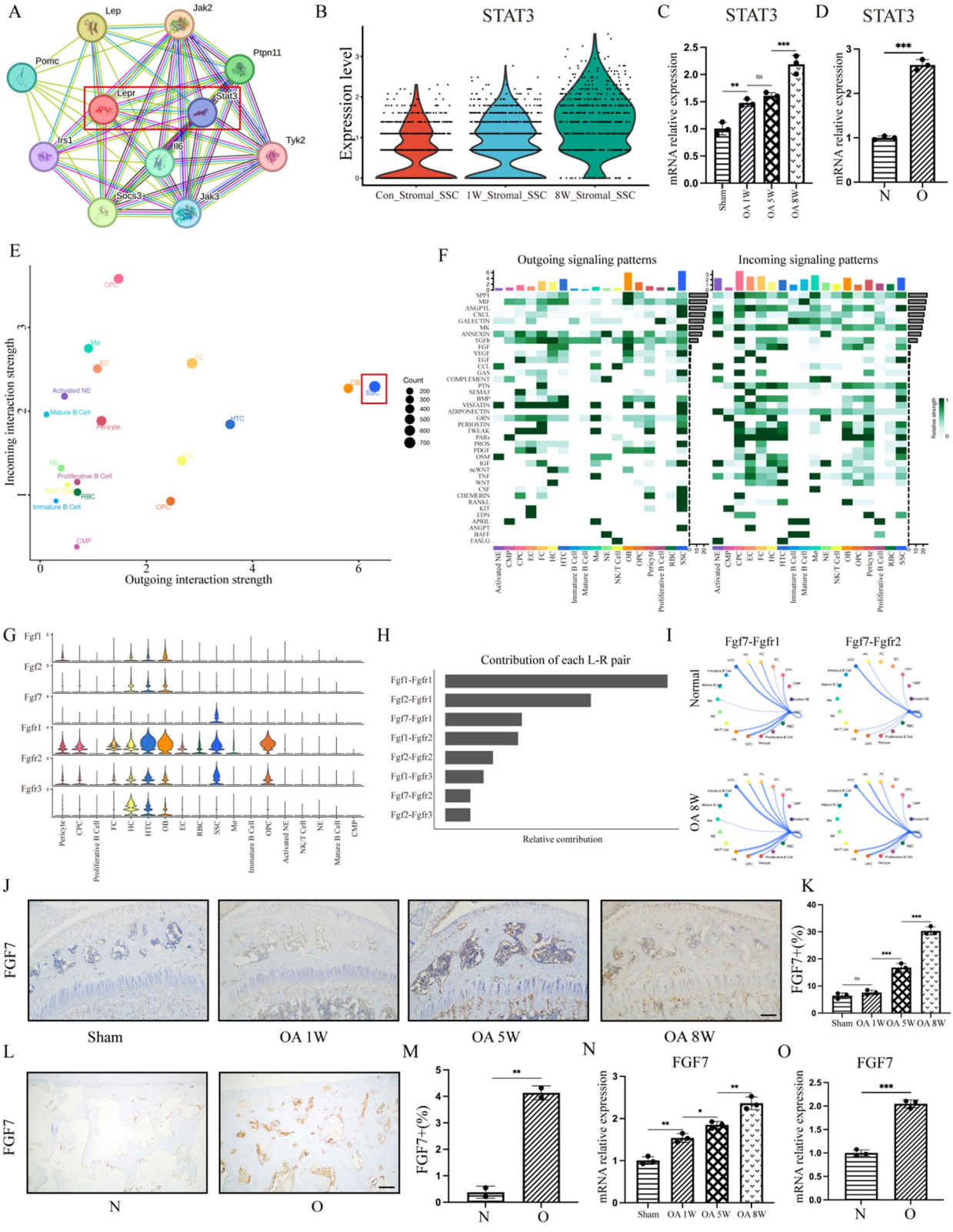

Fig. 4 (See legend on previous page.)

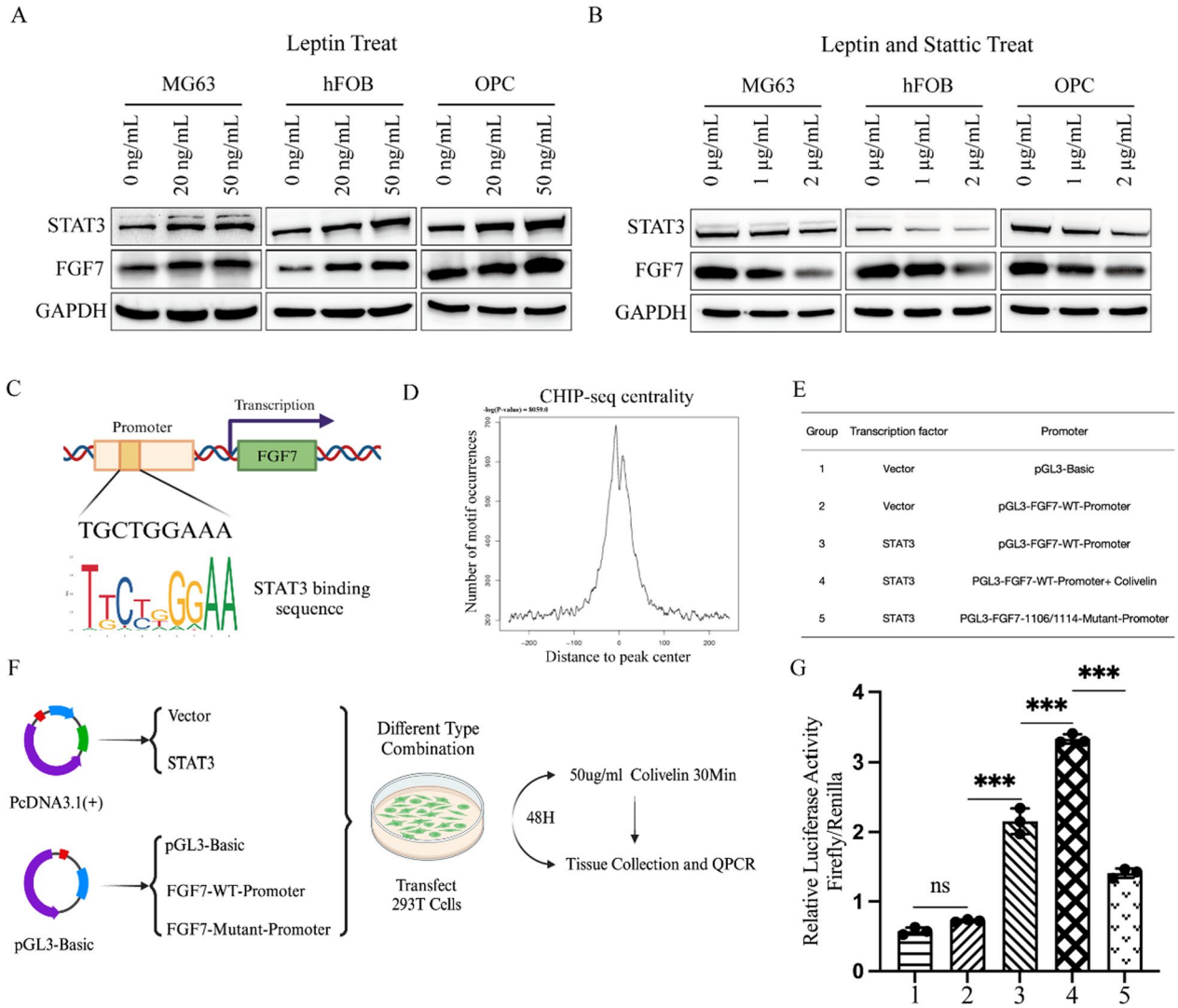

Fig. 5 The leptin-Lepr signaling pathway enhances expression of FGF7 via STAT3 activation. **A** Western blot analysis of the levels of STAT3 and FGF7 in MG63, hFOB, and OPC cells following leptin treatment. **B** Western blot analysis of STAT3 and FGF7 in MG63, hFOB, and OPC cells following treatment with leptin and Stattic. **C** The STAT3 binding site was predicted in the region of the FGF7 promoter by JASPAR. **D** ChIP-seq peaks used to identify motifs. **E** Luciferase assay group information. **F** Schematic of the luciferase assay regimen. **G** Luciferase activity in different groups. All data are presented as the mean ± S.D. **P* < 0.05; ***P* < 0.01; ****P* < 0.001; ns, not significant

(See figure on next page.)

Fig. 6 FGF7 regulated bone remodeling during OA progression. **A**, **B** Schematic of the treatment regimen (n = 3). **C** Knee articular cartilage safranin O/Fast Green staining in various treatment groups. Scale bar, 100 μm. **D** Representative images of COL II IHC in the articular cartilage and subchondral bone of various treatment groups. Scale bar, 100 μm. **E** Representative fluorescence images of Sp7-Cre/ERT2-Td knee joints with DAPI staining. **F** TRAP staining image of tibial subchondral bone and trabecular bone. Scale bar, 100 μm. **G** OARSI grade of the knee articular cartilage. **H** Quantitative analysis of the COL II area in articular cartilage and subchondral bone. **I**, **J** qPCR analysis of the expression levels of FGF7, RUNX2, SP7, Cx43, COL1a1, and SPP1 in various treatment groups. **K** Micro-CT scans of knee joints from various treatment groups after ALCT surgery. **L**, **M** Microarchitectures of tibial subchondral bones showing BV/TV (**L**) and Tb.Sp (**M**). Quantitative analyses were conducted using the IHC Profiler plug-in for ImageJ. All data are presented as the mean ± S.D. **P* < 0.05; ***P* < 0.01; ****P* < 0.001; ns, not significant

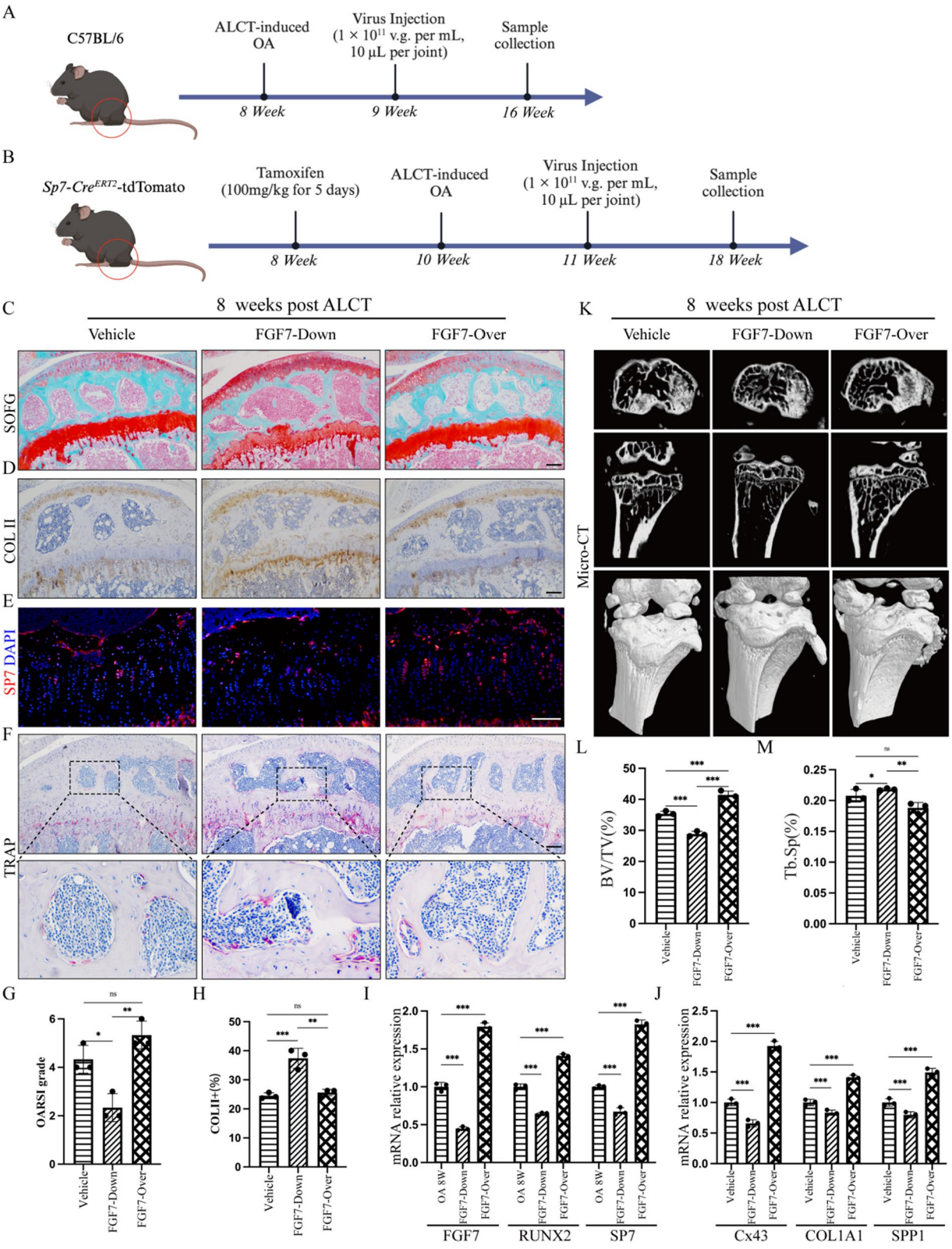

Fig. 6 (See legend on previous page.)

Sp7-Cre/ERT2-Td mice to substantiate our previous findings (Fig. 6B). The results of the IF analysis indicated that FGF7 increased the expression level of SP7 in OA (Fig. 6E). In addition to affecting bone formation, FGF7 was found to exert an inhibitory effect on osteoclast formation and bone resorption both in vitro and in vivo (Fig. 6F and S5C). Micro-CT analysis demonstrated that, compared with that in the vehicle treatment, FGF7 knockdown markedly diminished the BV/TV in the tibial subchondral bone. Conversely, FGF7 overexpression resulted in an increase in BV/TV (Fig. 6K, L). Moreover, trabecular separation (Tb.Sp) exhibited the opposite trend across distinct AAV treatments (Fig. 6K, M).

The aforementioned results revealed that during the progression of OA, FGF7 overexpression enhances bone formation and suppresses bone resorption, which may provide insight into a novel therapeutic strategy for OA.

Discussion

In the present study, the heterogeneity of cellular senescence in the synovium, articular cartilage, and subchondral bone of osteoarthritic joints was revealed by scRNA and functional analyses, and SSCs in subchondral bones were found to undergo senescence during OA progression. In addition, we showed that the activation of leptin-Lepr signaling resulted in SSC senescence and contributed to osteoarthritic lesions. The results of mechanistic explorations demonstrated that leptin-Lepr signaling induced expression of STAT3, which augmented the transcription of FGF7. Further in vivo and in vitro studies revealed that FGF7 exacerbated abnormal bone remodeling in the subchondral bones of osteoarthritic knee joints. Encouragingly, blockade of leptin-Lepr signaling and FGF7 using AAV or specific inhibitors partially alleviated SSC senescence and OA progression.

Cellular senescence has emerged as a mechanism that could be targeted to delay the osteoarthritic process. However, senescent cells exhibit varying degrees of susceptibility to senolytics, which suggests that even senescent cells are highly heterogeneous. With technological advancements, single-cell RNA-seq methods have emerged as one powerful tool for accurately identifying and characterizing senescent cells. Numerous studies have explored senescence heterogeneity in multiple tissues at the single-cell/nuclear level. Ogrodnik et al. demonstrated that both $p16^+$ and $p21^+$ cells accumulated more in microglia, oligodendrocyte progenitor cells, and oligodendrocytes in the hippocampus of aged mice [36], with remarkable heterogeneity, by performing single-nucleus RNA-seq and single-cell RNA-seq as well as in vivo animal analysis. Omori et al. reported the identification of $p16^+$ cells by single-cell RNA-seq in the liver and kidney of healthy and nonalcoholic steatohepatitis mouse livers [37]. The results showed that the distribution of $p16^+$ cells is highly heterogeneous among different organs and pathological conditions. Notably, recent studies have taken advantage of known senescence gene lists to identify senescent cells and determine novel cell subsets expressing senescence markers other than p16 and p21. Crespo-Garcia et al. identified a subset of senescent endothelial cells in the retina that highly express Col1a1, and functional data showed that this subset can be specifically eliminated by senolytic drugs [38]. OA has proven to be a whole-joint disease, and few single-scale analyses of cellular senescence are available, which limits the development and application of precise senescent elimination therapies for OA. Our study provides novel information concerning the heterogeneity of cellular senescence in osteoarthritic joints at the single-cell scale and reveals that $Lepr^+$ SSCs undergo senescent activity during OA progression, which is potentially helpful for understanding cellular senescence-mediated pathological processes and developing novel strategies to alleviate osteochondral lesions in OA joints.

Leptin has previously been reported to regulate cellular senescence in multiple tissues and to be involved in disease processes, including ovarian senescence, insulin resistance in type 2 diabetes, and obesity-associated neuropsychiatric disorders. Hense et al. reported that obesity induced by leptin deficiency increased the load of senescent cells in the ovary and was reduced by treatment with senolytics [39]. In addition, Rouault et al. reported that senescence-associated β-galactosidase (SA-β-gal) activity was positively associated with serum leptin and that senolytic treatment reduced SA-β-gal staining and normalized pathological alterations [40]. Moreover, Ogrodnik and colleagues found that the clearance of senescent cells from high fat-fed or Lepr-deficient obese mice restored neurogenesis and alleviated anxiety-related behavior [41]. In addition to metabolism-associated conditions, accumulating evidence suggests that leptin may promote cell senescence in skeletal tissues and contribute to bone lesions. Zhao et al. reported that activation of the leptin pathway by high expression of the long form of the Lepr (Ob-Rb) accelerated chondrocyte senescence in human OA samples [42]. In addition, high doses of leptin decreased the ability of rat chondrogenic progenitor cells to migrate, inhibited their chondrogenic potential, and increased their osteogenic potential [43]. However, little information about the effects of leptin on SSCs during OA progression is available. In the present study, leptin directly induced the senescence of SSCs in vivo and increased the number of senescent SSCs in the subchondral bones of PTOA model mice. Encouragingly, blockade

of leptin-mediated signaling significantly alleviated SSC senescence and osteoarthritic lesions in vivo, which proved that tissue-specific stem cells in skeletons can be candidate targets in leptin-induced bone disorders.

Although our findings and those of previous studies have demonstrated that senescent cells, including stem cells and differentiated cells, contribute to bone disorders and that targeting these cells alleviates pathological processes, the data have focused mainly on the regenerative capacity of cells for tissue repair. In the present study, the scRNA data and functional analysis revealed that senescent SSCs release considerable quantities of FGF7, a novel SASP that exacerbates bone remodeling in subchondral bones, which has not been previously revealed in OA conditions. FGF7 has been previously identified in numerous pathological conditions including thymocyte progenitor aging, muscle cell aging and regeneration, and pediatric hypophosphatasia progression [44–46]. In addition, FGF7 plays a more significant role in the bone development and homeostasis [47–50]. Mechanistic studies showed that FGF7 facilitates cell–cell communication through connexin43 and protects osteoblasts against oxidative damage through targeting mitochondria [35]. In the current study, FGF7 enhanced osteogenic differentiation of SSC and inhibited osteoclastogenesis, which indicating a novel role of senescent SSC in regulating subchondral bone remodeling. Most interestingly, FGF7 blockage in PTOA mice have demonstrated the translational valure of FGF7 targeting strategy.

We must acknowledge that present study has several limitations. First, scRNA-seq may miss capturing cells that are large or sensitive to dissociation because some senescent cells due to their enlarged size and physical fragility. Second, more OA models, such as aging OA, or collagenase-induced OA, need to be explored in future studies. Finally, although the findings that leptin-Lepr pathway and FGF7 blockage are potentially useful for developing novel molecular therapy on OA but in vivo studies in human being is indispensible.

Conclusion

Herein, scRNA-seq technology was employed to elucidate the cellular senescence of the synovium, articular cartilage, and subchondral bone from the knee joints of PTOA model mice. $Lepr^{+}$ SSCs in subchondral bones undergo cellular senescence during the progression of OA. Intra-articular injection of a leptin-Lepr chemical inhibitor and Lepr-targeting AAV inhibited SSC senescence in subchondral bone, which subsequently alleviated osteochondral lesions during OA progression. scRNA-seq analysis and molecular experimental data revealed that leptin induces STAT3 expression in SSCs and that STAT3 further binds to the FGF7 promoter region to promote its expression. Further intra-articular injection of FGF7-over- and FGF7-down AAV resulted in an overactive or suppressed bone remodeling phenotype, respectively, in the subchondral bone of PTOA mice. Direct addition of FGF7 to the cell culture system in vitro enhanced the osteogenic differentiation of SSCs while inhibiting osteoclast formation. Our data suggest that the leptin-Lepr pathway contributes to SSC senescence during OA progression and identifies FGF7 as a novel SASP factor for senescent SSCs, which may be helpful in the development of novel molecular therapies for OA.

In summary, our study revealed the heterogeneity of cellular senescence in OA joints, and identified an important role of Leptin-Lepr pathway for SSC senescence and OA progression via acting STAT3 thereafter inducing FGF7 expression, which worsening the abnormal subchondral bone remodeling. Our findings may shed light on the development of OA therapeutic strategies via blocking leptin-Lepr mediated pathological process.

Abbreviations

AAV	Adeno-associated virus
ALCT	Anterior cruciate ligament transection
ALP	Alkaline phosphatase
Bglap	Bone gamma-carboxyglutamate protein
BMP	Bone morphogenetic protein
BV/TV	Bone volume fraction
Cdkn1a	Cyclin-dependent kinase inhibitor 1A
Cdkn2a	Cyclin-dependent kinase inhibitor 2A
Cdh5	Cadherin 5
CPC	Cartilage progenitor cells
Col II	Collagen type II
CXCL	C-X-C Motif Chemokine Ligand
DEG	Differentially expressed genes
EC	Endothelial cells
FBS	Fetal bovine serum
FC	Fibroblasts
FGFR	Fibroblast growth factor receptor
FGF7	Fibroblast growth factor 7
Grem1	Gremlin 1
GO	Gene ontology
GSEA	Gene set enrichment analysis
IHC	Immunohistochemistry
IF	Immunofluorescence
IL-1β	Interleukin-1β
IL-6	Interleukin-6
KEGG	Kyoto Encyclopedia of Genes and Genomes
Lepr	Leptin receptor
OB	Osteoblast
OA	Osteoarthritis
OPC	Osteoblast progenitor cells
PBS	Phosphate-buffered saline
P53	Cellular tumor antigen p53
Prrx1	Paired related homeobox 1
PTOA	Post-traumatic osteoarthritis
RUNX2	Runt-related transcription factor 2
SASP	Senescence-associated secretory phenotype

SBP.th	Subchondral bone plate thickness
scRNA-seq	Single-Cell RNA sequencing
SSC	Skeletal stem cell
SP7	Specificity protein 7
SPP1	Secreted phosphoprotein 1
STAT3	Signal transducer and activator of transcription 3
Tb.Sp	Trabecular separation
TNFAIP3	Tumor Necrosis Factor Alpha-Induced Protein 3
TRAP	Tartrate-resistant acid phosphatase
UMAP	Uniform manifold approximation and projection

Supplementary Information

The online version contains supplementary material available at https://doi.org/10.1186/s13287-025-04342-1.

Additional file1 (DOCX 10599 KB)

Acknowledgements
The authors declare that they have not use AI-generated work in this manuscript.

Author contributions
Conceiving and designing experiments: Fu-Hao Yu, Bo-Feng Yin; Conduct the experiment: Fu-Hao Yu, Ming-Yu Liu,Wen-Jing Zhang, Xiao-Tong Li, Run-Xiang Xu; Provided technical assistance: Zhi-Dong Zhao, Xiao-Tong Li, Pei-Lin Li, Zhi-Ling Li; Performed the data analysis: Fu-Hao Yu; Offered valuable advice and strategies: Li Ding, Heng Zhu; visualization: Fu-Hao Yu; reviewed and revised the manuscript: Li Ding, Heng Zhu; Drafted the manuscript: Fu-Hao Yu, Heng Zhu.

Funding
This work was supported by the National Natural Sciences Grants China (Grant Nos. 82372373, 82172388), National Key R&D Program of China (Grant Nos. 2022YFA1104100, 2022YFA1103500), and the Beijing Natural Sciences Foundation (Grant No. 7222123, L212065).

Availability of data and materials
The raw sequence data reported in this paper have been deposited in the Genome Sequence Archive (Genomics, Proteomics & Bioinformatics 2021) in National Genomics Data Center (Nucleic Acids Res 2022), China National Center for Bioinformation / Beijing Institute of Genomics, Chinese Academy of Sciences (GSA: CRA019301). The data has been publicly shared and accessible at https://ngdc.cncb.ac.cn/gsa.

Declarations

Ethics approval and consent to participate
The animal research involved in this work was approved by the Institutional Animal Care and Use Committee of Military Medical Sciences. Title of the approved project: National Science Foundation for "The regulatory effects of chondrogenic progenitor cells on the osteoclast formation and bone remodeling in osteoarthritis". The initial Ethics approval (Approval No: IACUC-DWZX-2024-P523) was obtained on February 27, 2024. The care and use of animals were performed strictly following the regulations on the management of experimental animals. The research on human tibia plateau specimens samples involved in this work was approved by the Institutional Review Board at the Chinese People's Liberation Army General Hospital Title of the approved project: "discarded biological material from knee osteoarthritis patients with total knee arthroplasty for scientific research projects", The initial Ethics approval (2018-03-15) was obtained on March 15, 2018.

Competing interests
The authors declare that they have no competing interests.

Author details
[1]Department of Stem Cells and Regenerative Medicine, Beijing Institute of Radiation Medicine, Road Taiping 27, Beijing 100850, People's Republic of China. [2]Beijing Key Laboratory for Radiobiology, Beijing Institute of Radiation Medicine, Beijing 100850, People's Republic of China. [3]Department of Hematology, Air Force Medical Center, Fourth Military Medical University, Road Fucheng 30, Beijing 10142, People's Republic of China. [4]Graduate School, Fourth Military Medical University, Xi'an 710032, Shaanxi Province, People's Republic of China. [5]People's Liberation Army General Hospital, Road Fuxing 28, Beijing 100853, People's Republic of China. [6]School of Life Sciences, Hebei University, Baoding, People's Republic of China. [7]Anhui Medical University, Hefei, People's Republic of China.

Received: 6 December 2024 Accepted: 11 April 2025
Published online: 05 May 2025

References

1. Frydendal T, Christensen R, Mechlenburg I, Mikkelsen LR, Varnum C, Graversen AE, Kjaersgaard-Andersen P, Revald PH, Hofbauer C, Bieder MJ, et al. Total hip replacement or resistance training for severe hip osteoarthritis. N Engl J Med. 2024;391:1610–20. https://doi.org/10.1056/NEJMoa2400141.
2. Sharma L. Osteoarthritis of the knee. N Engl J Med. 2021;384:51–9. https://doi.org/10.1056/NEJMcp1903768.
3. Hunter DJ, Bierma-Zeinstra S. Osteoarthritis. Lancet. 2019;393:1745–59. https://doi.org/10.1016/S0140-6736(19)30417-9.
4. Jing Y, Jiang X, Ji Q, Wu Z, Wang W, Liu Z, Guillen-Garcia P, Esteban CR, Reddy P, Horvath S, et al. Genome-wide CRISPR activation screening in senescent cells reveals SOX5 as a driver and therapeutic target of rejuvenation. Cell Stem Cell. 2023;30(1452–1471): e1410. https://doi.org/10.1016/j.stem.2023.09.007.
5. Childs BG, Gluscevic M, Baker DJ, Laberge RM, Marquess D, Dananberg J, van Deursen JM. Senescent cells: an emerging target for diseases of ageing. Nat Rev Drug Discov. 2017;16:718–35. https://doi.org/10.1038/nrd.2017.116.
6. Jeon OH, Kim C, Laberge RM, Demaria M, Rathod S, Vasserot AP, Chung JW, Kim DH, Poon Y, David N, et al. Local clearance of senescent cells attenuates the development of post-traumatic osteoarthritis and creates a pro-regenerative environment. Nat Med. 2017;23:775–81. https://doi.org/10.1038/nm.4324.
7. Chen X, Gong W, Shao X, Shi T, Zhang L, Dong J, Shi Y, Shen S, Qin J, Jiang Q, Guo B. METTL3-mediated m(6)A modification of ATG7 regulates autophagy-GATA4 axis to promote cellular senescence and osteoarthritis progression. Ann Rheum Dis. 2022;81:87–99. https://doi.org/10.1136/annrheumdis-2021-221091.
8. Coryell PR, Diekman BO, Loeser RF. Mechanisms and therapeutic implications of cellular senescence in osteoarthritis. Nat Rev Rheumatol. 2021;17:47–57. https://doi.org/10.1038/s41584-020-00533-7.
9. Kang D, Shin J, Cho Y, Kim HS, Gu YR, Kim H, You KT, Chang MJ, Chang CB, Kang SB, et al. Stress-activated miR-204 governs senescent phenotypes of chondrocytes to promote osteoarthritis development. Sci Transl Med. 2019. https://doi.org/10.1126/scitranslmed.aar6659.
10. Zeng Q, Gong Y, Zhu N, Shi Y, Zhang C, Qin L. Lipids and lipid metabolism in cellular senescence: Emerging targets for age-related diseases. Ageing Res Rev. 2024;97: 102294. https://doi.org/10.1016/j.arr.2024.102294.
11. Zhu Y, Tchkonia T, Pirtskhalava T, Gower AC, Ding H, Giorgadze N, Palmer AK, Ikeno Y, Hubbard GB, Lenburg M, et al. The Achilles' heel of senescent cells: from transcriptome to senolytic drugs. Aging Cell. 2015;14:644–58. https://doi.org/10.1111/acel.12344.
12. Yousefzadeh MJ, Zhu Y, McGowan SJ, Angelini L, Fuhrmann-Stroissnigg H, Xu M, Ling YY, Melos KI, Pirtskhalava T, Inman CL, et al. Fisetin is a senotherapeutic that extends health and lifespan. EBioMedicine. 2018;36:18–28. https://doi.org/10.1016/j.ebiom.2018.09.015.
13. Ji ML, Jiang H, Li Z, Geng R, Hu JZ, Lin YC, Lu J. Sirt6 attenuates chondrocyte senescence and osteoarthritis progression. Nat Commun. 2022;13:7658. https://doi.org/10.1038/s41467-022-35424-w.
14. Cao H, Yang P, Liu J, Shao Y, Li H, Lai P, Wang H, Liu A, Guo B, Tang Y, et al. MYL3 protects chondrocytes from senescence by inhibiting clathrin-mediated endocytosis and activating of Notch signaling. Nat Commun. 2023;14:6190. https://doi.org/10.1038/s41467-023-41858-7.
15. Swahn H, Li K, Duffy T, Olmer M, D'Lima DD, Mondala TS, Natarajan P, Head SR, Lotz MK. Senescent cell population with ZEB1 transcription factor as its main regulator promotes osteoarthritis in cartilage and

meniscus. Ann Rheum Dis. 2023;82:403–15. https://doi.org/10.1136/ard-2022-223227.
16. Melis S, Trompet D, Chagin AS, Maes C. Skeletal stem and progenitor cells in bone physiology, ageing and disease. Nat Rev Endocrinol. 2024. https://doi.org/10.1038/s41574-024-01039-y.
17. Chan CKF, Gulati GS, Sinha R, Tompkins JV, Lopez M, Carter AC, Ransom RC, Reinisch A, Wearda T, Murphy M, et al. Identification of the human skeletal stem cell. Cell. 2018;175(43–56): e21. https://doi.org/10.1016/j.cell.2018.07.029.
18. He J, Yan J, Wang J, Zhao L, Xin Q, Zeng Y, Sun Y, Zhang H, Bai Z, Li Z, et al. Dissecting human embryonic skeletal stem cell ontogeny by single-cell transcriptomic and functional analyses. Cell Res. 2021;31:742–57. https://doi.org/10.1038/s41422-021-00467-z.
19. Li XT, Li ZL, Li PL, Wang FY, Zhang XY, Wang YX, Zhao ZD, Yin BF, Hao RC, Mao N, et al. TNFAIP3 derived from skeletal stem cells alleviated rat osteoarthritis by inhibiting the necroptosis of subchondral osteoblasts. Stem Cells. 2024;42:360–73. https://doi.org/10.1093/stmcls/sxad097.
20. Wang K, Li J, Li Z, Wang B, Qin Y, Zhang N, Zhang H, Su X, Wang Y, Zhu H. Chondrogenic progenitor cells exhibit superiority over mesenchymal stem cells and chondrocytes in platelet-rich plasma scaffold-based cartilage regeneration. Am J Sports Med. 2019;47:2200–15. https://doi.org/10.1177/0363546519854219.
21. Li ZL, Li XT, Hao RC, Wang FY, Wang YX, Zhao ZD, Li PL, Yin BF, Mao N, Ding L, Zhu H. Human osteoarthritic articular cartilage stem cells suppress osteoclasts and improve subchondral bone remodeling in experimental knee osteoarthritis partially by releasing TNFAIP3. Stem Cell Res Ther. 2023;14:253. https://doi.org/10.1186/s13287-023-03411-7.
22. Zhu H, Yang F, Tang B, Li XM, Chu YN, Liu YL, Wang SG, Wu DC, Zhang Y. Mesenchymal stem cells attenuated PLGA-induced inflammatory responses by inhibiting host DC maturation and function. Biomaterials. 2015;53:688–98. https://doi.org/10.1016/j.biomaterials.2015.03.005.
23. Li PL, Chen DF, Li XT, Hao RC, Zhao ZD, Li ZL, Yin BF, Tang J, Luo YW, Wu CT, et al. Microgel-based carriers enhance skeletal stem cell reprogramming towards immunomodulatory phenotype in osteoarthritic therapy. Bioact Mater. 2024;34:204–20. https://doi.org/10.1016/j.bioactmat.2023.12.022.
24. Tilg H, Ianiro G, Gasbarrini A, Adolph TE. Adipokines: masterminds of metabolic inflammation. Nat Rev Immunol. 2024. https://doi.org/10.1038/s41577-024-01103-8.
25. Liu Z, Xie W, Li H, Liu X, Lu Y, Lu B, Deng Z, Li Y. Novel perspectives on leptin in osteoarthritis: focus on aging. Genes Dis. 2024;11: 101159. https://doi.org/10.1016/j.gendis.2023.101159.
26. Karsenty G, Khosla S. The crosstalk between bone remodeling and energy metabolism: a translational perspective. Cell Metab. 2022;34:805–17. https://doi.org/10.1016/j.cmet.2022.04.010.
27. Dodington DW, Desai HR, Woo M. JAK/STAT: emerging players in metabolism. Trends Endocrinol Metab. 2018;29:55–65. https://doi.org/10.1016/j.tem.2017.11.001.
28. Shen B, Tasdogan A, Ubellacker JM, Zhang J, Nosyreva ED, Du L, Murphy MM, Hu S, Yi Y, Kara N, et al. A mechanosensitive peri-arteriolar niche for osteogenesis and lymphopoiesis. Nature. 2021;591:438–44. https://doi.org/10.1038/s41586-021-03298-5.
29. Hu H, Luo S, Lai P, Lai M, Mao L, Zhang S, Jiang Y, Wen J, Zhou W, Liu X, et al. ANGPTL4 binds to the leptin receptor to regulate ectopic bone formation. Proc Natl Acad Sci U S A. 2024;121: e2310685120. https://doi.org/10.1073/pnas.2310685120.
30. Elefteriou F, Ahn JD, Takeda S, Starbuck M, Yang X, Liu X, Kondo H, Richards WG, Bannon TW, Noda M, et al. Leptin regulation of bone resorption by the sympathetic nervous system and CART. Nature. 2005;434:514–20. https://doi.org/10.1038/nature03398.
31. Xie Y, Zinkle A, Chen L, Mohammadi M. Fibroblast growth factor signalling in osteoarthritis and cartilage repair. Nat Rev Rheumatol. 2020;16:547–64. https://doi.org/10.1038/s41584-020-0469-2.
32. Lazarus JE, Hegde A, Andrade AC, Nilsson O, Baron J. Fibroblast growth factor expression in the postnatal growth plate. Bone. 2007;40:577–86. https://doi.org/10.1016/j.bone.2006.10.013.
33. Qiu L, Cai J, Zhang N, Ma L, Fan FY, Li XM. Effect of miR-381-3p/FGF7 axis on the osteogenic differentiation of bone marrow mesenchymal stem cells through MEK/ERK signaling pathway. Tissue Cell. 2022;76: 101791. https://doi.org/10.1016/j.tice.2022.101791.
34. Liu X, Bai M, Sun Y, Hu X, Wang C, Xie J, Ye L. FGF7-induced E11 facilitates cell-cell communication through connexin43. Int J Biol Sci. 2021;17:3862–74. https://doi.org/10.7150/ijbs.65240.
35. Liu X, Hu X, Niu C, Yang Y, Huang Z, Xie J. Fibroblast growth factor 7 protects osteoblasts against oxidative damage through targeting mitochondria. FASEB J. 2024;38: e23524. https://doi.org/10.1096/fj.202301650RR.
36. McGinnis CS, Murrow LM, Gartner ZJ. DoubletFinder: doublet detection in single-cell RNA sequencing data using artificial nearest neighbors. Cell Syst. 2019;8(329–337): e324. https://doi.org/10.1016/j.cels.2019.03.003.
37. Hao Y, Stuart T, Kowalski MH, Choudhary S, Hoffman P, Hartman A, Srivastava A, Molla G, Madad S, Fernandez-Granda C, Satija R. Dictionary learning for integrative, multimodal and scalable single-cell analysis. Nat Biotechnol. 2024;42:293–304. https://doi.org/10.1038/s41587-023-01767-y.
38. Trapnell C, Cacchiarelli D, Grimsby J, Pokharel P, Li S, Morse M, Lennon NJ, Livak KJ, Mikkelsen TS, Rinn JL. The dynamics and regulators of cell fate decisions are revealed by pseudotemporal ordering of single cells. Nat Biotechnol. 2014;32:381–6. https://doi.org/10.1038/nbt.2859.
39. Jin S, Guerrero-Juarez CF, Zhang L, Chang I, Ramos R, Kuan CH, Myung P, Plikus MV, Nie Q. Inference and analysis of cell-cell communication using Cell Chat. Nat Commun. 2021;12:1088. https://doi.org/10.1038/s41467-021-21246-9.
40. Ogrodnik M, Evans SA, Fielder E, Victorelli S, Kruger P, Salmonowicz H, Weigand BM, Patel AD, Pirtskhalava T, Inman CL, et al. Whole-body senescent cell clearance alleviates age-related brain inflammation and cognitive impairment in mice. Aging Cell. 2021;20: e13296. https://doi.org/10.1111/acel.13296.
41. Omori S, Wang TW, Johmura Y, Kanai T, Nakano Y, Kido T, Susaki EA, Nakajima T, Shichino S, Ueha S, et al. Generation of a p16 reporter mouse and its use to characterize and target p16(high) cells in vivo. Cell Metab. 2020;32(814–828): e816. https://doi.org/10.1016/j.cmet.2020.09.006.
42. Crespo-Garcia S, Tsuruda PR, Dejda A, Ryan RD, Fournier F, Chaney SY, Pilon F, Dogan T, Cagnone G, Patel P, et al. Pathological angiogenesis in retinopathy engages cellular senescence and is amenable to therapeutic elimination via BCL-xL inhibition. Cell Metab. 2021;33(818–832): e817. https://doi.org/10.1016/j.cmet.2021.01.011.
43. Hense JD, Garcia DN, Isola JV, Alvarado-Rincon JA, Zanini BM, Prosczek JB, Stout MB, Mason JB, Walsh PT, Brieno-Enriquez MA, et al. Senolytic treatment reverses obesity-mediated senescent cell accumulation in the ovary. Geroscience. 2022;44:1747–59. https://doi.org/10.1007/s11357-022-00573-9.
44. Rouault C, Marcelin G, Adriouch S, Rose C, Genser L, Ambrosini M, Bichet JC, Zhang Y, Marquet F, Aron-Wisnewsky J, et al. Senescence-associated beta-galactosidase in subcutaneous adipose tissue associates with altered glycaemic status and truncal fat in severe obesity. Diabetologia. 2021;64:240–54. https://doi.org/10.1007/s00125-020-05307-0.
45. Ogrodnik M, Zhu Y, Langhi LGP, Tchkonia T, Kruger P, Fielder E, Victorelli S, Ruswhandi RA, Giorgadze N, Pirtskhalava T, et al. Obesity-induced cellular senescence drives anxiety and impairs neurogenesis. Cell Metab. 2019;29:1233. https://doi.org/10.1016/j.cmet.2019.01.013.
46. Zhao X, Huang P, Li G, Lv Z, Hu G, Xu Q. Activation of the leptin pathway by high expression of the long form of the leptin receptor (Ob-Rb) accelerates chondrocyte senescence in osteoarthritis. Bone Joint Res. 2019;8:425–36. https://doi.org/10.1302/2046-3758.89.BJR-2018-0325.R2.
47. Liu XY, Li X, Bai MR, Chen X, Wang CL, Xie J, Ye L. FGF-7 dictates osteocyte cell processes through beta-catenin transduction. Sci Rep. 2018;8:14792. https://doi.org/10.1038/s41598-018-33247-8.
48. Berent-Maoz B, Montecino-Rodriguez E, Signer RA, Dorshkind K. Fibroblast growth factor-7 partially reverses murine thymocyte progenitor aging by repression of Ink4a. Blood. 2012;119:5715–21. https://doi.org/10.1182/blood-2011-12-400002.
49. Ma L, Meng Y, An Y, Han P, Zhang C, Yue Y, Wen C, Shi X, Jin J, Yang G, Li X. Single-cell RNA-seq reveals novel interaction between muscle satellite cells and fibro-adipogenic progenitors mediated with FGF7 signalling. J Cachexia Sarcopenia Muscle. 2024;15:1388–403. https://doi.org/10.1002/jcsm.13484.
50. Whyte MP, Zhang F, Wenkert D, Mumm S, Berndt TJ, Kumar R. Hyperphosphatemia with low FGF7 and normal FGF23 and sFRP4 levels in the circulation characterizes pediatric hypophosphatasia. Bone. 2020;134: 115300. https://doi.org/10.1016/j.bone.2020.115300.